DOI: 10.1002/ejic.201001190

Tailor-Made Modification of a Gold Surface for the Chemical Binding of a High-Activity [FeFe] Hydrogenase

Henning Krassen,[a,b] Sven T. Stripp,*[c,d] Nadine Böhm,[e] Albrecht Berkessel,[e] Thomas Happe,[c] Kenichi Ataka,[a,d,f] and Joachim Heberle[a,d]

Keywords: Hydrogen / Metalloenzymes / Immobilization / Electrochemistry / IR spectroscopy

Hydrogenases are iron–sulfur proteins that catalyze hydrogen turnover in a wide range of microorganisms. Three different classes have been described, and among these [FeFe] hydrogenases are the most active in H_2 evolution. Hydrogenases are redox enzymes that have been shown to exchange electrons with graphite and modified noble metal electrodes. Making use of the latter, diffusible electron carriers are required to enable redox catalysis, as proteins do not specifically bind to the electrode surface. Diffusion-limited electron transfer can be replaced by electron injection into immobilized hydrogenase by binding the redox mediator to the electrode surface. Here, we present the synthesis and spectroelectrochemical characterization of 1-(10-mercaptodecyl)-1′-benzyl-4,4′-bipyridinium dibromide (MBBP), which is used as redox-active linker. *Cr*HydA1, the high-activity [FeFe] hydrogenase from *Chlamydomonas reinhardtii*, is immobilized on the linker-modified gold electrode. Each surface modification step is controlled in situ by surface-enhanced infrared absorption spectroscopy (SEIRAS). Functionality of the electrode–protein hybrid is demonstrated by recording the linker-supported current. The specific catalytic rate of hydrogen evolution by *Cr*HydA1 (2.9 $\mu mol\,H_2\,min^{-1}\,mg^{-1}$ hydrogenase) promises a valuable approach for further optimization of this novel bioelectrical interface.

1. Introduction

Many microorganisms developed enzymatic strategies to either consume or generate molecular hydrogen (H_2). Although H_2 is scarce in the earth's troposphere, anaerobic environments can show considerable concentrations. Some bacteria and archaea make use of H_2 uptake to power their energy balance,[1,2] while the great majority of hydrogen-processing microorganisms release H_2 as a product of proton recombination with excess reducing equivalents.[3] Evolution of H_2 is typical for strict and facultative anaerobes, since O_2 is not available as terminal electron acceptor under the given environmental conditions.[4,5]

A class of redox enzymes known as "hydrogenases" is mostly responsible for hydrogen turnover. These ancient iron–sulfur proteins are grouped into [NiFe], [FeFe], and Fe-only hydrogenases, depending on the transition metal composition of their active site.[6] [FeFe] hydrogenases are capable of catalyzing the release of H_2 at a rate of up to 1000 $\mu mol\,H_2\,min^{-1}\,mg^{-1}$.[7,8] Such high activity of H_2 production attracted significant interest for biotechnological and bio-inspired applications.

All [FeFe] hydrogenases share the same catalytic cofactor but differ in terms of molecular weight, amino acid sequence, and iron–sulfur cluster configuration. Hydrogen is activated at the characteristic prosthetic group, the six-iron "H-cluster". This cofactor comprises a [4Fe-4S] cluster, cysteine-bound to the catalytically active [2Fe-2S] moiety commonly referred to as "$[2Fe]_H$".[10] A serious obstacle in exploiting [FeFe] hydrogenases for biotechnological applications is their pronounced sensitivity to O_2,[11,12] Despite this obstacle, [FeFe] hydrogenases are attractive bio-catalysts, because of their outstanding efficiency in H_2 production, minimal liability to product inhibition, and overall structural integrity.

We have explored the possibility to develop an electrochemical interface to control the enzymatic activity of [FeFe] hydrogenases by immobilization on a gold electrode. We chose the hydrogenase of the green algae *Chlamydomonas reinhardtii* (*Cr*HydA1), which is one of the smallest [FeFe] hydrogenases known.[13,14] Furthermore, the enzyme

[a] Bielefeld University, Department of Chemistry, Biophysical Chemistry,
33615 Bielefeld, Germany
[b] Uppsala University, Department of Photochemistry and Molecular Science,
75120 Uppsala, Sweden
[c] Ruhr-Universität Bochum, Lehrstuhl Biochemie der Pflanzen, AG Photobiotechnologie,
44801 Bochum, Germany
[d] Freie Universität Berlin, Department of Physics, Experimental Molecular Biophysics,
14195 Berlin, Germany
[e] Universität zu Köln, Department für Chemie, Institut für Organische Chemie,
50939 Cologne, Germany
[f] Japan Science and Technology Agency,
102-0075, Tokyo, Japan
Supporting information for this article is available on the WWW under http://dx.doi.org/10.1002/ejic.201001190.

is remarkably active in H_2 evolution, insensitive to high salt concentration and high temperature, and displays comparatively moderate O_2 tolerance.[15,16] In our previous work, we showed that *Cr*HydA1 binds to a carboxy-terminated gold surface and H_2 production is induced by electron transfer through methyl viologen.[17] Armstrong and co-workers published the electrochemical characterization of a wide variety of [NiFe] and [FeFe] hydrogenases as adsorbed on pyrolytic graphite electrodes (see Vincent et al. for a review[18]), including that of *Cr*HydA1 of *C. reinhardtii*.[19,20] Hambourger et al. showed H_2 release with the [FeFe] hydrogenase of *Ca*HydA of *Clostridium acetobutylicum* on carbon felt electrodes,[21] and Baffert et al. investigated the O_2 sensitivity of the same enzyme.[8]

Spectroscopic methods are a complementary approach to investigate the mechanisms of hydrogen turnover at the atomic level. In order to fully exploit the advantages of both techniques, we make use of in situ surface-enhanced infrared absorption spectroscopy (SEIRAS), which combines highly sensitive IR spectroscopy with electrochemical control of the bound enzyme layer when a gold thin film is chosen as working electrode. In contrast to graphite, hydrogenases do not spontaneously adsorb on a bare gold surface if the latter is not chemically modified to enhance its affinity for protein binding. Such modification yields a tailor-made surface that optimizes the immobilization of the chosen protein.

In a recent approach, we showed that *Cr*HydA1 can exchange electrons with the electrode via an electron mediator (methyl viologen, Figure 1b) when immobilized on a carboxy-terminated gold electrode.[22] This chemically modified surface was capable to bind *Cr*HydA1 on the electrode, but direct electron transfer was not achieved. Although methyl viologen is an effective electron shuttle, the diffusion-limited migration between the gold surface and the enzyme layer essentially hampers the study of the enzymatic mechanism, in particular when time-resolved experiments are performed for kinetics studies.

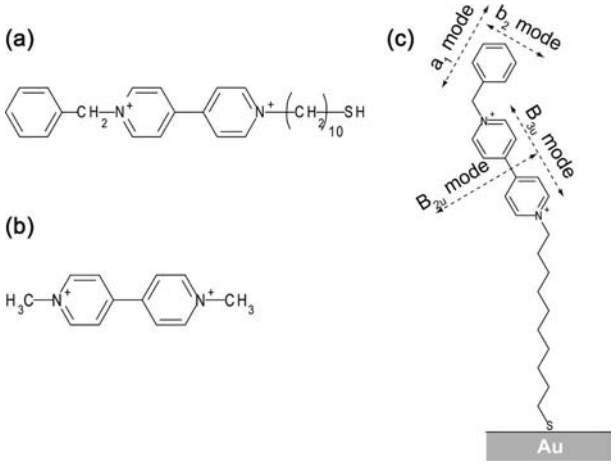

Figure 1. Chemical structures of (a) 1-(10-Mercaptodecyl)-1′-benzene-4,4′-bipyridinium dibromide (MBBP) and (b) methyl viologen. (c) Adsorption model of MBBP on a gold surface. Dashed arrows denote direction of net-dipole of each vibrational mode.

Here, we immobilize the electron mediator between electrode and enzyme. The [FeFe] hydrogenase of *C. reinhardtii* is deposited on a gold electrode by means of a newly synthesized linker thiol, namely 1-(10-mercaptodecyl)-1′-benzyl-4,4′-bipyridinium dibromide (MBBP, Figure 1b). The hydrogenase binds to this chemically modified gold surface with high affinity and receives reducing equivalents from the electrode. Because MBBP is redox-active, the presence of a soluble mediator is not required. We characterize the structure of the MBBP self-assembled monolayer (SAM) by SEIRAS. SEIRAS has been successfully applied to a whole variety of redox active proteins, including cytochrome c,[23] cytochrome c oxidase,[24] and both photosystems.[25,26] We follow the spontaneous formation of the hydrogenase monolayer and present a quantification of the amount of protein bound to the MBBP layer. Electron transfer and H_2 production activity of the immobilized hydrogenase is probed by protein film electrochemistry and gas chromatography.

2. Results

a. Surface Structure of the MBBP Monolayer

Figure 2a shows a SEIRA spectrum of MBBP adsorbed on a gold surface after 60 min of incubation. Positive bands represent the species adsorbed on the gold surface, while negative bands represent the species that disappeared from the surface during the adsorption process. There are nine positive bands observed in the region between 1800 and 1200 cm^{-1}. These bands are assigned to vibrational modes of MBBP. A broad negative-band peak around 1645 cm^{-1} is assigned to the H–O–H bending mode of water molecules expelled from the surface during the adsorption of MBBP. The bands at 1640, 1507, 1454, and 1365 cm^{-1} are assigned to the in-plane vibrational mode of the bipyridyl ring.[27] By assuming the terminal phenyl ring and the mercaptodecyl group as point mass, the bipyridyl group can be classi-

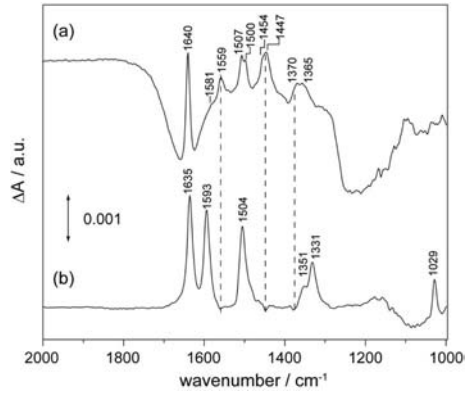

Figure 2. (a) SEIRA spectra of a MBBP self-assembled monolayer in oxidized state after binding in water solution. (b) The potential induced difference SEIRA spectrum of MBBP taken between 0.1 V (as reference, negative bands, oxidized state) and –0.4 V (as sample, positive bands, reduced state).

fied to the D_{2h} point group, since the molecule is centrosymmetric and planar in structure.

All bands in the observed spectral region are assigned to the B_{2u} or B_{3u} modes.[28,29] The bands at 1640 and 1507 cm^{-1} are assigned to the B_{3u} mode of the bipyridyl ring and ring and δ(CH) vibration, respectively.[30] The bands at 1454 and 1365 cm^{-1} are assigned to either the B_{2u} mode of the bipyridyl ring or the δ(CH) vibration. The B_{3u} mode comprises the dipole vector that goes along with its molecular axis, while the dipole vector of the B_{2u} mode is perpendicular to it (Figure 1c).[29] The experimental observation of both modes suggests that the molecular axis of the bipyridyl rings is tilted normal to the surface, according to the surface selection rules of SEIRAS.[31] It should be noted that the recorded relative intensities of the B_{2u} to the B_{3u} mode are stronger than those observed in the alkyl-terminated viologens.[32] This suggests that the tilting angle of the bipyridyl rings of MBBP is larger than that of the alkyl terminated viologens.

The band at 1559 cm^{-1} is assigned to the in-plane vibrational mode of the terminal phenyl group, since this band is missing in the spectrum of other alkyl-terminated viologen SAMs.[33] Other vibrational bands that can be assigned to the terminal phenyl group appear weakly at 1581 cm^{-1} as a shoulder, and at 1500, 1447, and 1370 cm^{-1}. The monosubstituted terminal phenyl group is classified as the C_{2v} point group. Thus, bands at 1581 and 1500 cm^{-1} are assigned to the a_1 vibrational mode while bands at 1559, 1447, and 1370 cm^{-1} are assigned to the b_2 vibrational mode.[34] The larger relative intensity of b_2 in comparison with the a_1 mode suggests that the molecular axis of the terminal phenyl group is tilted away from the surface normal (Figure 1a).

Figure 2b shows the potential-induced difference spectrum of MBBP. The reference spectrum was taken at –0.1 V vs. NHE, where the adsorbed MBBP is mainly in the oxidized form. The potential was then shifted to –0.55 V, where most of the MBBP is reduced, and the sample spectrum was taken. Positive bands represent the spectrum of MBBP in the reduced form, while negative bands represent that of the oxidized MBBP layer. The one-electron reduction of $MBBP^{2+}$ induced a change of the bipyridyl moiety to the corresponding radical cation.[35] As a consequence, six bands arose at 1635, 1593, 1504, 1351, 1331, and 1029 cm^{-1} in the observed spectral range.[36] A positive band at 1635 cm^{-1} is assigned to the asymmetric in-plane ring vibration mode of the radical cation monomer, while other positive bands are assigned to the vibrational modes of the radical cation dimer with a plane-to-plane configuration linked by π-bonding. The bands of the dimer are assigned to the totally symmetric (A_g) ring mode under the assumption of D_{2h} symmetry. The A_g modes are normally IR-inactive in D_{2h} symmetry. However, formation of a radical cation dimer, which is the simplest interaction unit in a quasi-one-dimensional charge-transfer complex, activates these IR-forbidden modes by vibronic coupling.[37]

It should be noted that the bands attributed to oxidized MBBP (Figure 2a) are scarcely observed in the difference spectrum. This is due to the enormous intensity enhancement of the IR spectra of the radical cation compared to that of the oxidized form. The effect has been attributed to intramolecular charge transfer, in which electron transfer among the bipyridyl groups couples to a normal vibrational mode, thereby inducing an enhanced oscillation of its molecular dipole.[37] Since the peak position of the A_g modes are close to those of the B_{2u} or B_{3u} modes, enhanced positive bands from the A_g mode of the radical cation dominate the weak negative bands of the oxidized form.

Several weak negative bands are observed at 1559, 1447, and 1370 cm^{-1}. These bands are assigned to ring vibrations of the terminal phenyl group. These vibrations belong to b_2 modes and, since they decrease in intensity, it is likely to assume that the terminal phenyl group changes its orientation to align the molecular axis perpendicular to the surface after radical formation. A concomitant increase of the a_1 modes of the terminal group could not be observed, since they overlap with the A_g modes of the bipyridyl group.

Reorientation of the MBBP SAM is also suggested by a change in the CH_2 stretching region (around 2900 cm^{-1}, not shown). There is a slight increase in the bands at 2842 and 2918 cm^{-1}, assigned to CH_2 in-phase and out-of-phase stretching modes, respectively.[38] Appearance of these bands suggests a change in the alkyl chain structure during formation of the radical cation at the bipyridyl group.

b. Electrochemistry of the MBBP Monolayer

Figure 3a shows cyclic voltammograms of the MBBP SAM on a gold film electrode in 100 mM KP_i buffer (pH = 7.0) measured at different potential sweep rates, *v*. At low *v* (< 50 mV s^{-1}), oxidative (anodic) and reductive (cathodic) current peaks are observed at –0.1 V and –0.17 V vs. NHE, respectively. The current density (*j*) increases linearly with *v* (Figure 3b). This indicates that the observed current is a result of the electron transfer to the adsorbed species.[39] The surface coverage (Γ) of the MBBP monolayer is derived from integration of the oxidative and reductive current. The coverage is determined to be $\Gamma = 2.31 \pm 0.3 \times 10^{-10}$ mol cm^{-2} (with a molecular diameter of 42 $Å^2$). This is in good agreement with reported values ($1.8–4.5 \times 10^{-10}$ mol cm^{-2}) for related systems.[40,41]

As *v* increases, the positions of the oxidative and reductive peaks shift to more positive and more negative potentials, respectively. The peak potentials are plotted as a function of log *v* in Figure 3c. From the midpoint potential of the current peak at the lower sweep rate limit, the formal potential, $E^{0\prime}$, is determined to be at 0.135 V vs. NHE (denoted by a dashed line in Figure 3c). Oxidative and reductive potentials deviate from $E^{0\prime}$ by an amount that is greater than |0.2 V| at *v* values greater than 1 V s^{-1}. Thus, analysis of the peak potentials at these *v* values can provide kinetic parameters on electron transfer. Based on the Butler–Volmer formalities,[39,42] the transfer coefficients (α) are determined to 0.6 and 0.4 for reduction and oxidation, respectively. Although α is close to 0.5 (totally reversible

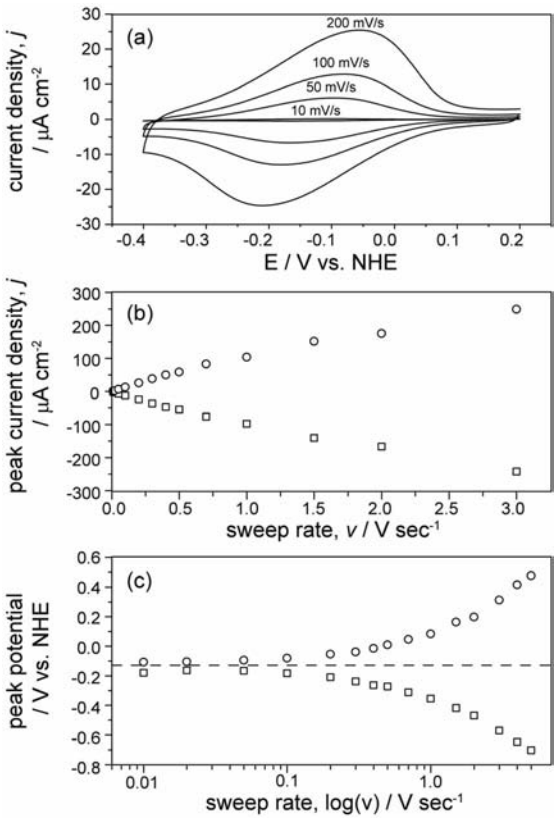

Figure 3. (a) Cyclic voltammograms of MBBP SAM on a gold electrode in 100 mM KP_i (pH = 7.0) recorded with potential sweep rates from 10 to 200 mV s^{-1} (T = 20 °C). (b) A plot of the peak current density as a function of the potential sweep rate for anodic (○) and cathodic (□) reaction. (c) A plot of the peak potentials as a function of the potential sweep rates for anodic (○) and cathodic (□) reaction.

reaction), the slight deviation from the ideal value suggests that electron transfer to and from MBBP is not totally equivalent. The uneven numbers of the transfer coefficient lead to the calculation of different rate constants for the reductive and oxidative electron transfer reactions. The determined standard electron transfer rate constants are 0.42 s^{-1} (reduction) and 0.96 s^{-1} (oxidation). This result somehow contradicts the former finding, which suggested that the redox reaction is fully reversible in a number of molecules involved in the surface reaction. However, the standard electron transfer rate constants suggest that additional reaction processes do not take place. The observed imbalance of transfer rates is explained by an intercalation of phosphate anions in the MBBP SAM. It has been suggested before that an intercalation of anionic molecules stabilizes the positive repulsive forces among the stacks of bipyridyl moieties in the fully oxidized form.[43,44] When the bipyridyl layer is reduced, these anions defuse away from the intercalated segments to maintain charge balance across the layer. The reduced bipyridyl layer forms dimeric charge-transfer structures as suggested from the IR spectra (vide supra). Hence, extra energy is necessary to remove the anions during electron transfer, which, consequently, selectively slows down the electron transfer rate in the reductive direction.

c. Adsorption of Hydrogenase on the Chemically Modified Electrode Surface

Adsorption of [FeFe] hydrogenase from *Chlamydomonas reinhardtii* on a MBBP-modified gold surface was followed in situ by SEIRAS. Figure 4a shows SEIRA spectra recorded during adsorption of *Cr*HydA1 on the MBBP SAM at open circuit potential (+0.2 V vs. NHE). Two prominent bands assigned to the protein backbone vibration are observed at 1654 and 1547 cm^{-1}.[45] The former band is assigned to the amide I mode, while the latter is assigned to the amide II mode of the protein backbone. The increase of the magnitude of these bands indicates an accumulation of *Cr*HydA1 protein at the surface. Besides these protein bands, a medium intense band is observed at 1403 cm^{-1}. Since this band appears in the positive direction, it is assigned to *Cr*HydA1. An intense band at this frequency has not been observed so far in other protein adsorption experiments on any other type of chemically modified surface. Although the amide III vibration typically appears at the corresponding region, a strong relative intensity as compared to the amide I and II bands is unlikely. An alternative interpretation for the 1403 cm^{-1} band includes the interaction of side-chain head groups of certain amino acid residues, which specifically interact with the MBBP SAM (possibly OH deformation vibration of serine, tyrosine or ring deformation of phenylalanine, histidine groups).[45] It is presumed that the strong interaction with MBBP causes retraction of these residues closer to the surface, which leads to stronger signal enhancement in SEIRAS. The existence of strong interaction is supported by the appearance

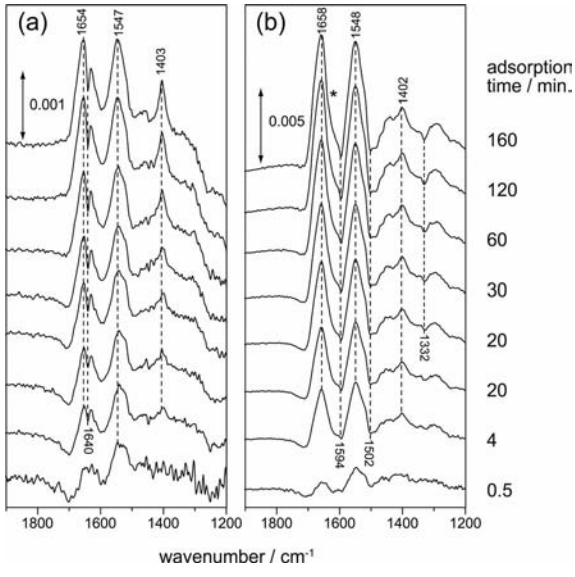

Figure 4. SEIRA spectra of *Cr*HydA1 adsorption on (a) oxidized (at open circuit potential, E_{OCP} = +0.2 V) and (b) reduced (at –0.2 V) MBBP-modified gold surface with various adsorption times.

of a sharp negative band at 1640 cm^{-1}, too. This band is assigned to the B_{3u} mode of the bipyridyl ring of the MBBP SAM (Figure 1c). The difference spectrum indicates a significant decrease of the 1640 cm^{-1} band, which means that the bipyridyl mode is altered upon adsorption of *Cr*HydA1.

Despite the changes in the bipyridyl vibrations, the bands of the terminal phenyl ring (1559 and 1447 cm^{-1} in Figure 2a) do not appear in the difference spectrum of Figure 4a. Hence, the terminal phenyl group was not affected by the binding of *Cr*HydA1. This result suggests that the bipyridyl group is more strongly influenced by the binding of protein than the terminal benzene group, although the latter is in immediate contact to the adsorbed protein.

As the surface charge might affect the adsorption process, we probed binding of *Cr*HydA1 to a reduced monolayer of MBBP (Figure 4b). It is evident that protein binding is more efficient at –0.2 V vs. NHE. Small but distinctive negative bands at 1594, 1502, and 1332 cm^{-1}, which appear concomitant to positive bands from the protein adsorption (amide I at 1658 and amide II at 1548 cm^{-1}), are assigned to the reduced MBBP. The observed MBBP bands are all assigned to the A_g mode of the bipyridyl rings. The A_g mode at 1635 cm^{-1} (see Figure 2b) of reduced MBBP is concealed by the overlap with the broad amide I band at 1658 cm^{-1} (see shoulder marked by an asterisk in Figure 4b). As already stated for the oxidized MBBP layer, this result suggests that *Cr*HydA1 adsorption is facilitated by strong interactions with the MBBP bipyridyl moiety.

It is peculiar that only the bands of the bipyridyl group are affected by the adsorption of *Cr*HydA1. It is not a possibility for the MBBP SAM layer to be partially desorbed during protein adsorption, because other vibrational fingerprints such as the bands of the terminal phenyl ring or the alkyl group remain untouched. An explanation for the sole change of the vibrational mode of the bipyridyl ring is a modulation of the absorption coefficient by protein binding. The relatively large absorption coefficient of the bipyridyl group in MBBP results from enhancement through intramolecular charge transfer, which is perturbed by adsorption of *Cr*HydA1. As a consequence, the absorption coefficient decreases and it is observed as a negative band, despite the fact that the surface concentration of MBBP remains constant.

d. SPR Measurements

The quantity of the adsorbed *Cr*HydA1 protein is assessed by surface plasmon resonance (SPR). 170 mg L^{-1} *Cr*HydA1 were injected into the measurement cell with a constant flow rate of 5 µL min^{-1} for 60 min. Then, the *Cr*HydA1 sample was flushed with buffer solution. A change in the response signal, ΔR, before and after the binding of *Cr*HydA1 is determined to be 2350 RUs (resonance units). Specifically bound *Cr*HydA1 is calculated to be 2.35 ng mm^{-2} (3.57×10^{-12} mol cm^{-2}) by using the conversion factor of 1000 RUs/ng mm^{-2}.[46,47] This value corresponds well to the previously observed value of 2.25 ng mm^{-2} for *Cr*HydA1 adsorption on a mercaptopropionic acid modified electrode.[48] The determined value is close to the theoretical monolayer value (2.3–4.6 ng *Cr*HydA1 mm^{-2}), calculated by assuming a surface area (23–47 nm^2 $molecule^{-1}$) of a homologous model structure using the catalytic subunit of *Cp*I hydrogenase from *Clostridium pasteurianum*.[49]

The monolayer coverage suggests that *Cr*HydA1 binds specifically to the MBBP layer and the adsorption ratio is calculated to correspond to one *Cr*HydA1 molecule bound per 150 MBBP molecules.

e. Hydrogen Evolution Activity

After binding of *Cr*HydA1 to the MBBP SAM layer, residual *Cr*HydA1 in the bulk solution was removed by buffer exchange. Then, the electrode potential was kept constant at –0.45 V vs. NHE for 85 min while the current was monitored by chronoamperometry. The steady-state current of H_2 evolution is –0.8 µA for the *Cr*HydA1/MBBP electrode (Figure 5a). The evolved H_2 gas was accumulated in a gastight 20 mL electrochemical cell. 1 mL of the gas phase was taken by a syringe and analyzed by gas chromatography. The amount of H_2 produced was calculated from integration of the peak at the retention time of H_2 (data not shown) and determined to be 208 nmol, corresponding to 2.4 ± 0.2 nmol H_2 min^{-1}. In combination with a surface

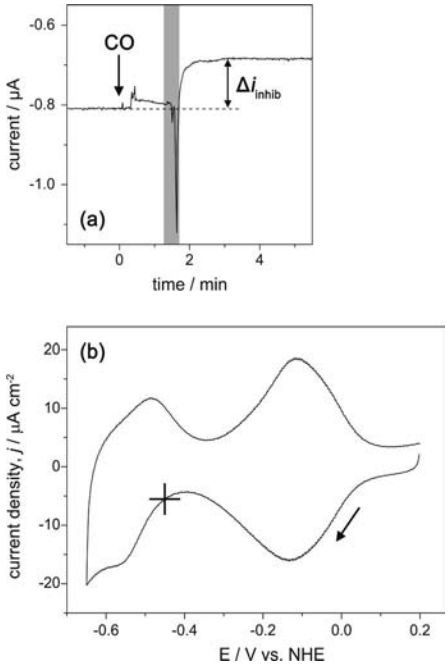

Figure 5. (a) Steady-state current from hydrogen evolution of *Cr*HydA1/MBBP electrode in 100 mM KP_i (pH = 7.0). A constant potential, E = –0.45 V vs. NHE, is applied to the electrode. At t = 0 min, 1 mL CO-saturated buffer is injected into the cell. After 75 s of the injection, the solution is stirred for 30 s as indicated by the shaded section. The experiment is conducted at T = 20 °C. (b) Cyclic voltammogram of a MBBP-coated gold electrode in 100 mM KP_i, pH = 7.0 (potential sweep rate = 50 mV s^{-1}, T = 20 °C). The arrow indicates the scanning direction. For illustration, the –0.45 V working potential is marked.

coverage of 3.57×10^{-12} mol cm^{-2}, the specific H_2 evolution activity of the enzyme is calculated to be 192 mol H_2 min^{-1} mol^{-1} *Cr*HydA1, or 2.9 μmol H_2 min^{-1} mg^{-1} *Cr*HydA1.

It should be noted that the steady-state current of H_2 evolution at –0.45 V vs. NHE contains an additional contribution from the MBBP layer. Figure 5b shows a cyclic voltammogram of the blank MBBP layer. Although H_2 evolution is catalyzed by MBBP only at potentials higher than –0.8 V, a considerable number of electrons are consumed in the reduction of the bipyridyl group at –0.45 V. In order to evaluate the catalytic contribution specifically from *Cr*HydA1, the amperometric current was probed by CO inhibition (Figure 5a). Initially, the potential was kept at –0.45 V and the H_2 evolution current was measured. At t = 0, 1 mL of CO-saturated buffer was injected into the electrolyte solution in the electrochemical cell. Following an incubation time of 75 s, the solution was stirred for 30 s to support diffusion of CO to the electrode. The steady-state reductive current specifically decreased by $\Delta i_{inhib} = 0.12$ μA. This drop in the H_2 evolution current is due the CO inhibition of *Cr*HydA1, suggesting that Δi originates from the catalytic activity of the hydrogenase enzyme. The inhibition constant k_{inhib} has been determined to be 8.0×10^{-4} s^{-1} μM^{-1} under reducing conditions (–0.4 V vs. NHE).[11] Hence, it is fair to assume that CO inhibition is complete in this experiment. Carbon monoxide is used as a specific inhibitor of hydrogenase activity and does not affect the redox activity of the MBBP layer.

Discussion

The newly established MBBP SAM has a high affinity for the [FeFe] hydrogenase *Cr*HydA1 and efficiently supports formation of a protein monolayer under the given conditions. Its bipyridyl group promotes electron transfer from the gold surface to the adsorbed enzyme without the need of a soluble mediator.

It is informative to compare the presented system to alternative methods of protein immobilization. *Cr*HydA1 adsorbed on PGE electrodes shows direct electron transfer[50] with only a slight infliction of the cyclic voltammogram at i = 0. Although the binding of a completely water-soluble, small, and almost globular protein is supposed to be random on PGE, the graphite surface allows for (1) close contact of the biomolecules without structural interference and (2) direct electron transfer as a function of the graphite roughness. However, the possibility of an orientated binding on PGE can not be ruled out conclusively.

These results provide a clue for the mechanism of electron transfer between *Cr*HydA1 and the assayed MBBP surface. The MBBP monolayer exposes a terminal phenyl ring towards the solution phase (Figure 1a). Two-dimensionally aligned structures of the phenyl rings provide a structure similar to the edge planes of pyrolytic graphite. The structural analogy of the phenyl ring layer to PGE potentially leads to a more favorable binding or orientation of *Cr*HydA1. The bipyridyl group of MBBP is located beneath the terminal phenyl group, bridging the "tunneling gap" in the middle of the molecule (Figure 1a), so electrons immediately travel the comparatively wide range between electrode and *Cr*HydA1 reaction center. It is presumed that the bipyridyl group of MBBP serves as electron relay at the midpoint of the long electron transfer pathway.

The H_2 evolution activity of the MBBP/*Cr*HydA1 system should be assessed by comparison to the established in vitro system, which is H_2 evolution activity without tethering to the electrode surface. The observed activity of the MBBP/*Cr*HydA1 electrode system, 2.9 μmol H_2 min^{-1} mg^{-1} *Cr*HydA1, is higher by a factor of two as compared to the previously reported value of MPA/*Cr*HydA1 with solubilized methyl viologen as mediator (1.28 μmol H_2 min^{-1} mg^{-1}).[51] Nevertheless, these activity values are far lower than the activity measured in solution. The H_2 evolution activity of *Cr*HydA1 in solution is determined by an in vitro test based on methyl viologen (see Experimental Section) to be 453 μmol H_2 min^{-1} mg^{-1} *Cr*HydA1. When MBBP is used as an electron mediator in solution, the in vitro H_2 evolution activity drops to 113 μmol H_2 min^{-1} mg^{-1}. This shows that the electrode-tethered MBBP/*Cr*HydA1 system reveals only 2.5% of the hydrogen evolution potential as suggested by the MBBP/*Cr*HydA1 in vitro test. Several factors are responsible for the diminished activity. (1) Although MBBP is bound to the electrode surface, the electron-accepting bipyridyl group is at a distance of about 20 Å from the electrode surface. This is due to the C_{10} alkyl chain (Figure 1a). The electron transfer rate is clearly slowed down by this separation. (2) The quasi-two-dimensional crystal structure formed by the stacked layer of bipyridyl groups involves an intercalation of anion species during vertical electron transfer, which further slows down the transfer of electrons. (3) Moreover, the two-dimensional stacking of the terminal phenyl groups forms a hydrophobic "finish", which prevents counteranions from compensating for the bipyridyl positive charge. These factors account for the slow electron transfer rate of 0.42–0.96 s^{-1} of the MBBP SAM layer.

In addition to slow electron transfer with the MBBP SAM as discussed above, a strong interaction between *Cr*HydA1 and MBBP may also explain the diminished apparent H_2 evolution activity. Although the high affinity of *Cr*HydA1 to the MBBP surface makes the enzyme bind in an orientation that allows for electron transfer, this arrangement should slightly deviate from the optimum conformation for electron transfer to the reaction center of *Cr*HydA1. As a consequence, the adsorbed protein has to be re-orientated to transfer electrons from MBBP to the reaction center. Such a re-orientation model was proposed to explain the slow electron transfer of cytochrome c or Azurin adsorbed on a chemically modified electrode surface.[52,53] A combination of all these factors slows down the entire turnover rate of the *Cr*HydA1 H_2 evolution reaction, eventually leading to the observed efficiency difference between the in solution assay and the activity of the tethered MBBP/*Cr*HydA1 system.

3. Conclusion

We present a novel modification procedure for gold surfaces allowing adsorption and electron transfer to the highly active [FeFe] hydrogenase from *Chlamydomonas reinhardtii* (*Cr*HydA1). We made use of MBBP, a tailor-made C_{10} thiol that carries a 4,4′-bipyridyl group and a benzene ring at the distal end, which mimic both methyl viologen as an electron relay and a graphite-like benzene "finish", respectively. The redox-active MBBP monolayer was characterized by IR spectroscopy (SEIRAS). Furthermore, the protein-binding process was followed in detail. We were able to judge the amount of hydrogenase enzyme bound by SPR and could estimate the specific H_2 evolution activity of the MBBP/*Cr*HydA1 electrode surface. The catalytic activity was probed by electrochemistry and gas chromatography. By combining these data, the specific H_2 evolution activity of the tethered MBBP/*Cr*HydA1 system was determined to 2.9 μmol H_2 min^{-1} mg^{-1} *Cr*HydA1 which is about 2.5% of what was suggested by the in vitro activity assay. We have discussed the reason for this drop in specific H_2 evolution activity in terms of the rate-limiting steps of electron transfer at the interface between the electrode and the active site of *Cr*HydA1.

4. Experimental Section

Purification of [FeFe] Hydrogenase from *Chlamydomonas reinhardtii*: Recombinant [FeFe] hydrogenase, *Cr*HydA1-$STII_{C-tag}$, was synthesized and purified as described before.[54] An optimized purification protocol was established. Ultracentrifugation and affinity chromatography on a 10 mL Strep-Tactin Superflow column (IBA, Göttingen, Germany) were applied. Cell growth and protein purification were carried out under strict anaerobic conditions. The isolated protein was concentrated to 5 g L^{-1} on Vivaspin 6-columns (Sartorius Stedim Biotech, Göttingen, Germany) and stored in 10% glycerol. In variation to the original protocol by von Abendroth et al., 150 mM NaCl was used with the Tris/HCl buffers.

Synthesis of *N*-Benzyl-4,4′-bipyridinium Bromide: A solution of 4,4′-bipyridine (1.5 g, 9.6 mmol, 1.3 equiv.) in dry acetone (50 mL) was placed into a 250 mL round-bottomed flask under argon and heated to reflux. A solution of benzyl bromide (900 mL, 7.38 mmol, 1.0 equiv.) was added in a dropwise manner. After approximately 60 min, a yellow-green precipitation occurred. After 2.5 h, the solvent was removed under reduced pressure. The remaining yellow-green solid was washed with diethyl ether and recrystallized from ethanol/diethyl ether (1:1) to afford 2.22 g (92%) of a yellowish solid, m.p. 224 °C. The analytical data were in agreement with the literature.[55]

Synthesis of 1-Acetylthio-10-bromodecane: Potassium thioacetate (2.5 g, 21.9 mmol, 1.0 equiv.) was dissolved under argon in abs. THF (180 mL). Under argon, this solution was added to a solution of 1,10-dibromodecane (9.8 g, 43.8 mmol, 2.0 equiv.) in abs. THF (20 mL) at room temperature. The mixture was then heated to reflux for 24 h. The precipitate was filtered off, and the solvent was removed from the filtrate at reduced pressure. The remaining semisolid was purified by silica gel chromatography (ethyl acetate/*n*-hexane, 1:10), affording 2.58 g (40%) of a colorless oil. The analytical data were in agreement with the literature.[56]

Synthesis of the *S*-Acetyl-Protected MBBP Linker: *N*-Benzyl-4,4′-bipyridium bromide (500 mg, 1.53 mmol, 1.0 equiv.) was dissolved in acetonitrile (20 mL). 1-Acetylthio-10-bromodecane (722 mg, 2.45 mmol, 1.6 equiv.) was added, and the mixture was heated at 80 °C for 120 h. A yellow precipitate formed, which was filtered off and washed with diethyl ether, affording 429 mg (45%) of the desired product as a yellow powder, m.p. >240 °C.

Synthesis of 1-(10-Mercaptodecyl)-1′-benzyl-4,4′-bipyridinium Dibromide (MBBP): In a Schlenk flask, the *S*-acetyl protected MBBP linker (100 mg, 160 μmol, 1.0 equiv.) was dissolved in abs. methanol (80 mL) under argon. The solution was cooled to –78 °C, and acetyl chloride (1.26 g, 16.06 mmol 110 equiv.) was slowly added with stirring. The reaction mixture was then warmed to room temperature, and stirring was continued at that temperature for 12 h. After concentration of the solution under reduced pressure, the MBBP linker was obtained in quantitative yield (93 mg) as a yellow solid, m.p. > 240 °C. See its characterization by NMR spectroscopy in the Supporting Information.

Surface Modification Monitored by Surface-Enhanced Infrared Absorption Spectroscopy (SEIRAS)

Details of the SEIRAS setup have already been described.[57] Briefly, a nanostructured gold thin film was chemically deposited on one side of a triangular silicon prism. A spectroelectrochemical cell was mounted on top of the prism. The infrared beam, provided by the interferometer of the FTIR spectrometer (Bruker Vertex 70, Bruker Optics, Ettlingen, Germany), was coupled into the single reflection silicon prism at an incident angle of 60°. The beam was totally internally reflected at the gold-coated prism side, and the intensity was measured by a mercury cadmium telluride (MCT) detector.

The bare gold surface was immersed for 60 min in an aqueous solution of MBBP. A reference IR spectrum of the solvent-covered surface was subtracted from a series of sample spectra, which were recorded after addition of the protein sample. After the self-assembled monolayer (SAM) of MBBP was formed, the surface was rinsed with the solvent several times and finally with sodium phosphate buffer solution (10 mM, pH 6.8) to remove the MBBP solution. The kinetics of immobilization of *Cr*HydA1 (3.5 μM) was monitored by recording spectra in time intervals of 10–60 s.

Cyclic Voltammetry

The gold film was not only employed as the plasmonic substrate for SEIRAS but concomitantly used as working electrode in a series of electrochemical experiments. Ag/AgCl and platinum mesh were used as reference and counter electrode, respectively. Cyclic voltammograms were recorded with a potentiostat (Autolab PGSTAT 12, Eco Chemie B.V., Utrecht, Netherlands). All potentials are reported vs. the normal hydrogen electrode (NHE) with the conversion $E_{NHE} = 0.2\ E_{Ag/AgCl}$ (in V) at room temperature. Cyclic voltammetry and chronoamperometry experiments were performed at ambient temperature (T = 20 °C), with KP_i (100 mM) buffer with pH = 7.0.

An anaerobic chamber (Coy Laboratory Products, Grassland, MI, USA) was used to provide an O_2-free environment for the electrochemical experiments. The N_2 atmosphere contained about 1% H_2, which reduced O_2 contaminants at a palladium catalyst within the chamber. All solutions were degassed for at least 30 min and stored in the anaerobic chamber for approximately two weeks prior to use. Equipment, transferred to the anaerobic chamber, was evacuated for at least 30 min. In this environment, the recorded cyclic voltammograms were stable, and the hydrogenase was not subject to O_2 inactivation during the measurement.

Amperometric H_2 Production: The modified gold surface was embedded in a home-made, gas-tight electrochemical cell with a total volume of 20 mL. The setup was purged with argon to remove the ambient H_2 of the anaerobic chamber. 1 mL of the gas phase in the measuring cell was injected into a gas chromatograph (GC-2010, Shimadzu, Kyoto, Japan) equipped with a PLOT fused silica-coated molsieves column (5 Å, 10 m by 0.32 mm; Varian, Palo Alto, CA) to gauge whether the H_2 atmosphere was completely exchanged. Ten minutes of exposure under an argon atmosphere was sufficient to yield a H_2-free gas phase. Then, a potential of –0.45 V vs. NHE was applied for 85 min while the current was monitored (100 mM KP_i, pH = 7.0, T = 20 °C). The amount of H_2 evolved was determined by injecting 1 mL of the extracted gas mixture from the electrochemical cell into the gas chromatograph.

Surface Plasmon Resonance (SPR): Surface plasmon resonance experiments were performed by using a Biacore 3000 (GE Healthcare, Uppsala, Sweden) with a constant flow rate of 5 $\mu L\,min^{-1}$. Gold sensor chips were used to provide a bare gold surface for each experiment. To form the SAM on the gold surface, an aqueous saturated MBBP solution (150 µL) was injected. For the immobilization of hydrogenase, the running buffer was changed from Millipore water to KP_i buffer (100 mM, pH = 6.8) and *Cr*HydA1 (300 µL with a final concentration of 170 $\mu g\,mL^{-1}$) were injected.

In Vitro Activity Assay: To probe H_2 evolution activity under optimal conditions, *Cr*HydA1 (1–10 µg) was added to a KP_i buffer solution (100 mM, 2 mL, pH = 6.8) containing methyl viologen or MBBP (1 mM) and sodium dithionite (100 mM). This solution was sealed gas-tight in an 8 mL SUBA tube, purged with argon, and incubated at 37 °C for 15 min. The amount of H_2 produced was measured by gas chromatography (as described above), and the specific H_2 evolution activity of the hydrogenase (in $\mu mol\,H_2\,min^{-1}\,mg^{-1}$ hydrogenase) was calculated.

Supporting Information (see footnote on the first page of this article): The ^1H and ^{13}C NMR spectroscopic characterization of 1-(10-mercaptodecyl)-1′-benzyl-4,4′-bipyridinium dibromide (MBBP).

Acknowledgments

This work was supported by a grant from Bundesministerium für Bildung und Forschung (BMBF) (Grundlagen für einen biotechnologischen und biomimetischen Ansatz der Wasserstoffproduktion). T. Happe was further supported by the Volkswagen foundation (LigH2t). K. Ataka was supported by the PRESTO program of the Japan Science and Technology Agency. We acknowledge these financial supports. We also thank Prof. N. Sewald and K. Wollschläger for use of the Biacore 3000 SPR device and discussions.

[1] R. Cramm, *J. Mol. Microbiol. Biotechnol.* **2009**, *16*, 38–52.
[2] K. Schütz, T. Happe, O. Troshina, P. Lindblad, E. Leitão, P. Oliveira, P. Tamagnini, *Planta* **2004**, *218*, 350–359.
[3] M. Stephenson, L. H. Stickland, *Biochem. J.* **1931**, *25*, 205–214.
[4] M. W. W. Adams, *Biochim. Biophys. Acta Bioenerg.* **1990**, *1020*, 115–145.
[5] A. Melis, L. P. Zhang, M. Forestier, M. L. Ghirardi, M. Seibert, *J. Plant Physiol.* **2000**, *122*, 127–135.
[6] J. C. Fontecilla-Camps, A. Volbeda, C. Cavazza, Y. Nicolet, *Chem. Rev.* **2007**, *107*, 4273–4303.
[7] L. Girbal, G. von Abendroth, M. Winkler, P. M. C. Benton, I. Meynial-Salles, C. Croux, J. W. Peters, T. Happe, P. Soucaille, *Appl. Environ. Microbiol.* **2005**, *71*, 2777–2781.
[8] C. Baffert, M. Demuez, L. Cournac, B. Burlat, B. Guigliarelli, P. Bertrand, L. Girbal, C. Leger, *Angew. Chem.* **2008**, *120*, 2082; *Angew. Chem. Int. Ed.* **2008**, *47*, 2052–2054.
[9] S. Stripp, O. Sanganas, T. Happe, M. Haumann, *Biochemistry* **2009**, *48*, 5042–5049.
[10] Y. Nicolet, C. Piras, P. Legrand, C. E. Hatchikian, J. C. Fontecilla-Camps, *Structure Fold. Des.* **1999**, *7*, 13–23.
[11] G. Goldet, C. Brandmayr, S. T. Stripp, T. Happe, C. Cavazza, J. C. Fontecilla-Camps, F. A. Armstrong, *J. Am. Chem. Soc.* **2009**, *131*, 14979–14989.
[12] S. T. Stripp, G. Goldet, C. Brandmayr, O. Sanganas, K. A. Vincent, M. Haumann, F. A. Armstrong, T. Happe, *Proc. Natl. Acad. Sci. USA* **2009**, *106*, 17331–17336.
[13] S. Stripp, O. Sanganas, T. Happe, M. Haumann, *Biochemistry* **2009**, *48*, 5042–5049.
[14] C. Kamp, A. Silakov, M. Winkler, E. J. Reijerse, W. Lubitz, T. Happe, *Biochim. Biophys. Acta Bioenerg.* **2008**, *1777*, 410–416.
[15] G. Goldet, C. Brandmayr, S. T. Stripp, T. Happe, C. Cavazza, J. C. Fontecilla-Camps, F. A. Armstrong, *J. Am. Chem. Soc.* **2009**, *131*, 14979–14989.
[16] T. Happe, J. D. Naber, *Eur. J. Biochem.* **1993**, *214*, 475–481.
[17] H. Krassen, S. Stripp, A. G. von, K. Ataka, T. Happe, J. Heberle, *J. Biotechnol.* **2009**, *142*, 3–9.
[18] K. A. Vincent, A. Parkin, F. A. Armstrong, *Chem. Rev.* **2007**, *107*, 4366–4413.
[19] G. Goldet, C. Brandmayr, S. T. Stripp, T. Happe, C. Cavazza, J. C. Fontecilla-Camps, F. A. Armstrong, *J. Am. Chem. Soc.* **2009**, *131*, 14979–14989.
[20] S. T. Stripp, G. Goldet, C. Brandmayr, O. Sanganas, K. A. Vincent, M. Haumann, F. A. Armstrong, T. Happe, *Proc. Natl. Acad. Sci. USA* **2009**, *106*, 17331–17336.
[21] M. Hambourger, M. Gervaldo, D. Svedruzic, P. W. King, D. Gust, M. Ghirardi, A. L. Moore, T. A. Moore, *J. Am. Chem. Soc.* **2008**, *130*, 2015–2022.
[22] H. Krassen, S. Stripp, A. G. von, K. Ataka, T. Happe, J. Heberle, *J. Biotechnol.* **2009**, *142*, 3–9.
[23] K. Ataka, J. Heberle, *J. Am. Chem. Soc.* **2004**, *126*, 9445–9457.
[24] K. Ataka, B. Richter, J. Heberle, *J. Phys. Chem. B* **2006**, *110*, 9339–9347.
[25] A. Badura, B. Esper, K. Ataka, C. Grunwald, C. Wöll, J. Kuhlmann, J. Heberle, M. Rögner, *Photochem. Photobiol.* **2006**, *82*, 1385–1390.
[26] H. Krassen, A. Schwarze, B. Friedrich, K. Ataka, O. Lenz, J. Heberle, *ACS Nano* **2009**, *3*, 4055–4061.
[27] A. Topacli, S. Akyuz, *Spectrochim. Acta Part A* **1995**, *51*, 633–641.
[28] G. Zerbi, S. Sandroni, *Spectrochim. Acta Part A* **1968**, *24*, 483.
[29] G. Zerbi, S. Sandroni, *Spectrochim. Acta Part A* **1968**, *24*, 511.
[30] A. Topacli, S. Akyuz, *Spectrochim. Acta Part A* **1995**, *51*, 633–641.
[31] M. Osawa, K. Ataka, K. Yoshii, Y. Nishikawa, *Appl. Spectrosc.* **1993**, *47*, 1497–1502.
[32] B. Han, Z. Li, T. Wandlowski, A. Blaszczyk, M. Mayor, *J. Phys. Chem. C* **2007**, *111*, 13855–13863.
[33] B. Han, Z. Li, T. Wandlowski, A. Blaszczyk, M. Mayor, *J. Phys. Chem. C* **2007**, *111*, 13855–13863.
[34] E. E. Ernstbrunner, R. B. Girling, R. E. Hester, *J. Chem. Soc. Faraday Trans. 2* **1978**, *74*, 1540–1549.
[35] X. Y. Tang, T. W. Schneider, J. W. Walker, D. A. Buttry, *Langmuir* **1996**, *12*, 5921–5933.
[36] S. H. R. Brienne, R. P. Cooney, G. A. Bowmaker, *J. Chem. Soc. Faraday Trans.* **1991**, *87*, 1355–1359.
[37] S. H. R. Brienne, P. D. W. Boyd, P. Schwerdtfeger, G. A. Bowmaker, R. P. Cooney, *J. Chem. Soc. Faraday Trans.* **1993**, *89*, 3015–3020.
[38] N. B. Colthup, L. H. Daly, S. E. Wiberley, *Introduction to Infrared and Raman Spectroscopy*, Academic Press, New York, **1990**.

[39] A. J. Bard, L. R. Faulkner, *Electrochemical Method: Fundamentals and Applications*, John Wiley & Sons, Inc., New York **1980**.
[40] B. Han, Z. Li, T. Wandlowski, A. Blaszczyk, M. Mayor, *J. Phys. Chem. C* **2007**, *111*, 13855–13863.
[41] X. Y. Tang, T. W. Schneider, J. W. Walker, D. A. Buttry, *Langmuir* **1996**, *12*, 5921–5933.
[42] E. Laviron, *J. Electroanal. Chem.* **1979**, *101*, 19–28.
[43] M. Osawa, K. Yoshii, *Appl. Spectrosc.* **1997**, *51*, 512–518.
[44] M. Osawa, W. Suetaka, *J. Electroanal. Chem.* **1989**, *270*, 261–272.
[45] S. Krimm, J. Bandekar, *Adv. Protein Chem.* **1986**, *38*, 181–364.
[46] S. H. Armstrong, M. J. E. Budka, K. C. Morrison, M. Hasson, *J. Am. Chem. Soc.* **1947**, *69*, 1747–1753.
[47] E. Stenberg, B. Persson, H. Roos, C. Urbaniczky, *J. Colloid Interf. Sci.* **1991**, *143*, 513–526.
[48] H. Krassen, S. Stripp, A. G. von, K. Ataka, T. Happe, J. Heberle, *J. Biotechnol.* **2009**, *142*, 3–9.
[49] J. W. Peters, W. N. Lanzilotta, B. J. Lemon, L. C. Seefeldt, *Science* **1998**, *282*, 1853–1858.
[50] G. Goldet, C. Brandmayr, S. T. Stripp, T. Happe, C. Cavazza, J. C. Fontecilla-Camps, F. A. Armstrong, *J. Am. Chem. Soc.* **2009**, *131*, 14979–14989.
[51] H. Krassen, S. Stripp, A. G. von, K. Ataka, T. Happe, J. Heberle, *J. Biotechnol.* **2009**, *142*, 3–9.
[52] L. J. Jeuken, *Biochim. Biophys. Acta Bioenerg.* **2003**, *1604*, 67–76.
[53] L. J. C. Jeuken, J. P. Mcevoy, F. A. Armstrong, *J. Phys. Chem. B* **2002**, *106*, 2304–2313.
[54] G. von Abendroth, S. Stripp, A. Silakov, C. Croux, P. Soucaille, L. Girbal, T. Happe, *Int. J. Hydrogen Energy* **2008**, *33*, 6076–6081.
[55] J. A. Barltrop, A. C. Jackson, *J. Chem. Soc. Perkin Trans. 2* **1984**, 367–371.
[56] D. I. Gittins, D. Bethell, R. J. Nichols, D. J. Schiffrin, *J. Mater. Chem.* **2000**, *10*, 79–83.
[57] K. Ataka, J. Heberle, *Anal. Bioanal. Chem.* **2007**, *388*, 47–54.
Received: November 11, 2010
Published Online: February 2, 2011

